Available online at www.sciencedirect.com
ScienceDirect
Trans. Nonferrous Met. Soc. China 30(2020) 756−764

Transactions of Nonferrous Metals Society of China
www.tnmsc.cn

# Dielectric properties and relaxor ferroelectric behavior of $(1-y)Ba(Zr_{0.1}Ti_{0.9})O_3-yBa(Zn_{1/3}Nb_{2/3})O_3$ ceramics

Xin ZHONG, Chen ZHANG, Fang-xu CHEN, Zhu-ming TANG, Gang JIAN

Department of Materials Science and Engineering, Jiangsu University of Science and Technology,
Zhenjiang 212003, China

Received 29 May 2019; accepted 24 December 2019

**Abstract:** The microstructure, dielectric and ferroelectric properties of $(1-y)Ba(Zr_{0.1}Ti_{0.9})O_3-yBa(Zn_{1/3}Nb_{2/3})O_3$ ($y$=0−0.05) ceramics prepared by traditional solid state method were investigated by X-ray diffractometer, scanning electron microscope, electric parameter testing system and ferroelectric tester. It is found that the barium zirconate titanate based ceramics are single-phase perovskites as $y$ increases up to 0.05 and their average grain size decreases with the increase of $y$. The permittivity maximum $\varepsilon_{r,max}$ is suppressed from 8948 to 1611 at 1 kHz with increasing $y$, and the ferroelectric−paraelectric phase transition temperature $T_m$ decreases from 93 to −89 °C at 1 kHz as $y$ increases. The composition-induced diffuse phase transition is enhanced with increasing $y$. The relaxor-like ferroelectric behavior with a strong frequency dispersion of $T_m$ and permittivity at $T<T_m$ accompanied by a strong diffuse phase transition is found for the system with high $y$ value. The remnant polarization decreases with increasing $y$, while the coercive field decreases remarkably and then increases with the increase of $y$.

**Key words:** barium zirconate titanate; dielectric properties; relaxor ferroelectric behavior; perovskite; phase transition

## 1 Introduction

The perovskite materials such as $BaTiO_3$, $Na_{0.5}Bi_{0.5}TiO_3$, $K_{0.5}Na_{0.5}NbO_3$ and $Nd_{1-x}Ba_xCoO_3$ are responsible for the development in modern technology to a great extent since they are a vital part of capacitors, pyroelectric detectors, ultrasound sensors, actuators and so forth [1−6]. Among them, barium zirconate titanate ($Ba(Ti_{1-x}Zr_x)O_3$, or BZT), the solid solution of $BaTiO_3$ and $BaZrO_3$, has received extensive attention for its potential applications in ceramic capacitors owing to its eminent dielectric performance [7−9].

$BaTiO_3$ goes through three phase transitions from cubic to tetragonal (at 120 °C), tetragonal to orthorhombic (at 5 °C) and orthorhombic to rhombohedral phase (at −90 °C) when cooling [10]. The permittivity ($\varepsilon_r$) normally reaches a maximum value at the ferroelectric to paraelectric phase transition temperature known as Curie temperature, $T_C$. Above $T_C$, the temperature dependence of permittivity follows the Curie−Weiss law. As the $Zr^{4+}$ ions occupy the central sites of oxygen octahedrons in $BaTiO_3$, the cubic−tetragonal phase transition temperature decreases and the tetragonal−orthorhombic phase transition temperature shifts towards higher value with increasing $Zr^{4+}$ content, leading to a pinched phase transition ($x<0.15$) [11]. For further substitution ($x>0.15$), only a rhombohedral−cubic phase transition takes place [12]. Also, the diffuse paraelectric−ferroelectric phase transition stimulated by increasing the amount of zirconium is noticed [13]. As $x$ approaches 0.3, the ferroelectric behavior of BZT system changes from a “normal” one to a typical relaxor one which mainly occurs in lead-based compositions with more than one type of ions occupying the equivalent

---

**Corresponding author:** Chen ZHANG; Tel: +86-511-84401184; Fax: +86-511-84407381; E-mail: czhang1981@hotmail.com

DOI: 10.1016/S1003-6326(20)65251-7

six-coordinated crystallographic sites. Although the strong diffuse paraelectric−ferroelectric phase transition of BZT relaxor ferroelectrics helps to improve temperature stability of permittivity, the low transition temperature, for example 198 K for $Ba(Ti_{0.7}Zr_{0.3})O_3$, results in a very low permittivity at room temperature, which restricts the real applications of the BZT ceramics with high Zr content in capacitors [14].

Trivalent rare earth cations (La, Dy, Sm, Eu, Y, Nd, etc) help to induce a relaxor-type behavior of BZT ceramics in a manner similar to the effects of an increment of zirconium [9,15−18]. Moreover, the diffusivity degree of phase transition increases due to both the increment of the lanthanide content and the increase of the ionic radius of the dopant element. The ytterbium dopant is found to enormously enhance and broaden the relative permittivity maximum of BZT ceramics with the increase of ytterbium content. A novel Y5V dielectric material with the room temperature dielectric constant over 23000 and the dielectric strength higher than 4.0 kV/mm under alternating current (AC) field is developed in the ytterbium-doped BZT ceramics [19]. The composites of the $Ba(Zr_{0.07}Ti_{0.93})O_3$ ceramic and the CoO nano-particles (1.0−3.0 vol.%) also show broad relative permittivity versus temperature ($\varepsilon_r-T$) curves with frequency dispersion [20]. However, less effort has been put into finding a balance between the fine temperature stability of permittivity and high permittivity at room temperature by introducing an analogous system with different aliovalent ions in the equivalent six-coordinated crystallographic sites in the BZT matrix. Therefore, the present study involves the modification in structural, dielectric and ferroelectric properties of $Ba(Zr_{0.1}Ti_{0.9})O_3$ matrix by successively adding $Ba(Zn_{1/3}Nb_{2/3})O_3$. The study highlights the effects of $Ba(Zn_{1/3}Nb_{2/3})O_3$ on dielectric parameters, phase transition and ferroelectric behavior of BZT ceramics to explore their potential for practical capacitor applications in bypassing or coupling circuits.

## 2 Experimental

The $(1-y)Ba(Zr_{0.1}Ti_{0.9})O_3-yBa(Zn_{1/3}Nb_{2/3})O_3$ ($y$=0, 0.01, 0.02, 0.03, 0.04 and 0.05) (short for BZT−BZN) specimens were synthesized by traditional solid state method. High purity $BaCO_3$ (>99.0%), $ZrO_2$ (>99.0%), $TiO_2$ (>98.0%), ZnO (>99.0%) and $Nb_2O_5$ (>99.0%) powders, namely the starting raw materials, were weighed according to Table 1. After being ball-milled in deionized water for 24 h, the slurries were dried and then the obtained mixtures were calcined in air at 1080 °C for 2 h. After calcination, the powders were reground and added with 5 wt.% polyvinyl alcohol (PVA) for granulation. Sintering was conducted in air at 1360 °C for 2 h after green pellets were obtained by die pressing under 250 MPa. For dielectric measurement, the specimens with BQ−5311 silver paste coated on the top and bottom surfaces were fired at 800 °C for 10 min.

**Table 1** Masses of raw materials for $(1-y)Ba(Zr_{0.1}Ti_{0.9})O_3-yBa(Zn_{1/3}Nb_{2/3})O_3$ ceramics

| $y$ | Mass of raw material/g | | | | |
|---|---|---|---|---|---|
| | $BaCO_3$ | $ZrO_2$ | $TiO_2$ | ZnO | $Nb_2O_5$ |
| 0 | 33.2313 | 2.0750 | 12.1048 | 0 | 0 |
| 0.01 | 33.1873 | 2.0515 | 11.9679 | 0.0456 | 0.1490 |
| 0.02 | 33.1433 | 2.0281 | 11.8313 | 0.0911 | 0.2976 |
| 0.03 | 33.0995 | 2.0047 | 11.6951 | 0.1365 | 0.4458 |
| 0.04 | 33.0558 | 1.9815 | 11.5593 | 0.1818 | 0.5937 |
| 0.05 | 33.0122 | 1.9582 | 11.4238 | 0.2269 | 0.7411 |

The crystalline structures of the ceramics were confirmed by X-ray diffraction analysis (XRD, Rigaku D/max 2500v/pc) with Cu $K_\alpha$ radiation at the step of 2 (°)/min. And the scanning electron microscope (JSM−6480 ESEM) was applied for observing the surface morphologies of the as-sintered specimens. The average grain size of BZT−BZN ceramics was calculated using the Nano Measurer software. The temperature dependence of dielectric parameters was measured at 200 Hz, 1 kHz, 10 kHz, 100 kHz, 250 kHz and 500 kHz from −180 to 230 °C with TZDM−200−300C automatic electric parameter measuring system. The polarization−electric field ($P-E$) hysteresis characteristics were obtained by utilizing the Radiant Precision Premier II ferroelectric tester.

## 3 Results and discussion

### 3.1 Crystal structure

Figure 1 shows the XRD patterns of as-sintered $(1-y)Ba(Zr_{0.1}Ti_{0.9})O_3-yBa(Zn_{1/3}Nb_{2/3})O_3$

bulk ceramics. All of the samples exhibit typical tetragonal perovskite structure (space group *P*4*mm*), without obvious evidence of the secondary phase, indicating that the present system is a single phase solid solution with $Ba^{2+}$ ion in the *A* site and aliovalent ions ($Zr^{4+}$, $Ti^{4+}$, $Zn^{2+}$ and $Nb^{5+}$) in the *B* site of perovskite structure even when *y* reaches up to 0.05.

### 3.2 Surface morphology

Figure 2 shows the surface morphologies of as-sintered $(1-y)Ba(Zr_{0.1}Ti_{0.9})O_3-yBa(Zn_{1/3}Nb_{2/3})O_3$ ceramics. It is obvious that all the samples exhibit dense microstructures and fine grain size distribution. The average grain size of BZT−BZN ceramics shown in Table 2 decreases obviously with the increase of $Ba(Zn_{1/3}Nb_{2/3})O_3$ content. In other words, the grain growth for pure $Ba(Zr_{0.1}Ti_{0.9})O_3$ ceramic is significantly inhibited after the combination with $Ba(Zn_{1/3}Nb_{2/3})O_3$.

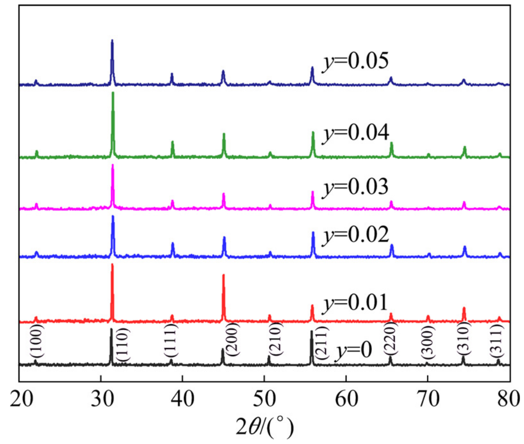

**Fig. 1** XRD patterns for $(1-y)Ba(Zr_{0.1}Ti_{0.9})O_3-yBa(Zn_{1/3}Nb_{2/3})O_3$ ceramics

### 3.3 Frequency characteristics

The temperature dependence of the relative dielectric constant and the dielectric loss for $(1-y)Ba(Zr_{0.1}Ti_{0.9})O_3-yBa(Zn_{1/3}Nb_{2/3})O_3$ ceramics at

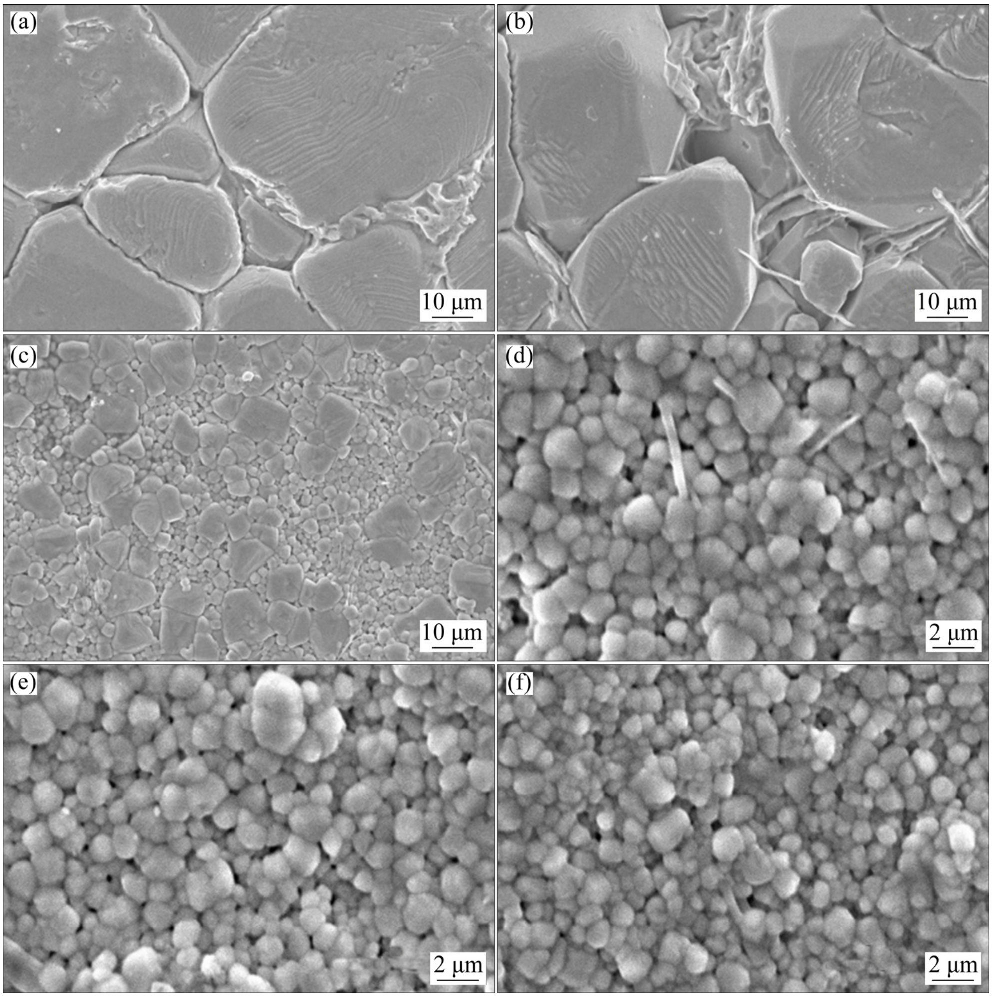

**Fig. 2** SEM micrographs of $(1-y)Ba(Zr_{0.1}Ti_{0.9})O_3-yBa(Zn_{1/3}Nb_{2/3})O_3$ ceramics: (a) $y$=0; (b) $y$=0.01; (c) $y$=0.02; (d) $y$=0.03; (e) $y$=0.04; (f) $y$=0.05

**Table 2** Average grain sizes of (1−$y$)Ba(Zr$_{0.1}$Ti$_{0.9}$)O$_3$−$y$Ba(Zn$_{1/3}$Nb$_{2/3}$)O$_3$ ceramics

| $y$ | 0 | 0.01 | 0.02 | 0.03 | 0.04 | 0.05 |
|---|---|---|---|---|---|---|
| Grain size/μm | 54.27 | 46.59 | 2.99 | 1.85 | 1.45 | 1.12 |

200 Hz, 1 kHz, 10 kHz, 100 kHz, 250 kHz and 500 kHz is shown in Fig. 3. All BZT−BZN ceramics possess the dielectric constant peaks corresponding to the ferroelectric−paraelectric phase transition in the temperature range from −180 to 230 °C. The maximum value of the dielectric permittivity is symbolized as $\varepsilon_{r,max}$ while using $T_m$ as the temperature corresponding to this permittivity maximum. As shown in Fig. 3(a), the relative dielectric constant of pure Ba(Zr$_{0.1}$Ti$_{0.9}$)O$_3$ ceramic remains almost same as the test frequency increases from 200 Hz to 500 kHz. Particularly, there is no frequency dispersion of the dielectric maximum $\varepsilon_{r,max}$ of the pure Ba(Zr$_{0.1}$Ti$_{0.9}$)O$_3$ ceramic. Also, as the test frequency increases, no shift in $T_m$ for

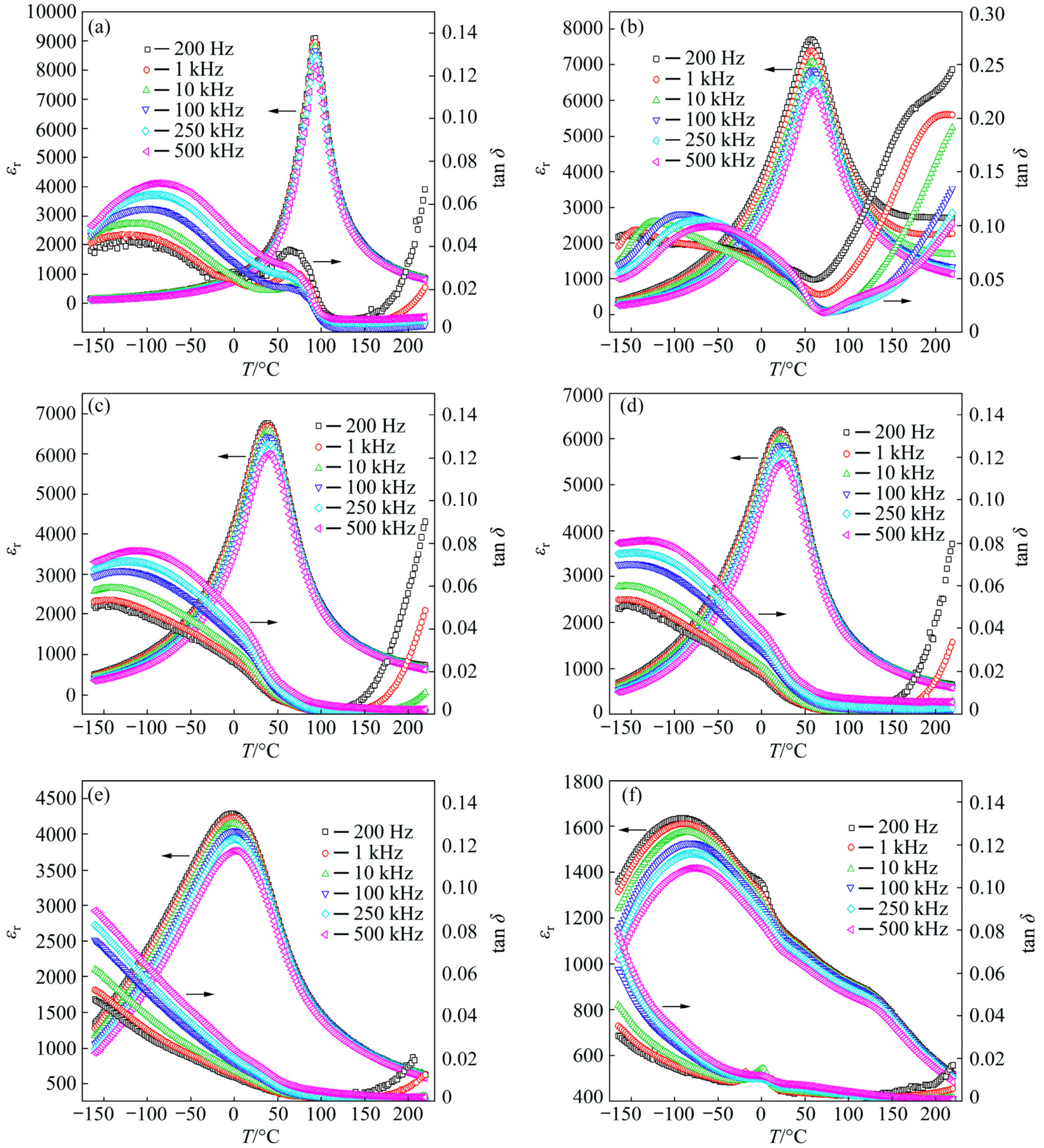

**Fig. 3** Temperature dependence of relative dielectric constant and dielectric loss for (1−$y$)Ba(Zr$_{0.1}$Ti$_{0.9}$)O$_3$−$y$Ba(Zn$_{1/3}$Nb$_{2/3}$)O$_3$ ceramics at different frequencies: (a) $y$=0; (b) $y$=0.01; (c) $y$=0.02; (d) $y$=0.03; (e) $y$=0.04; (f) $y$=0.05

$Ba(Zr_{0.1}Ti_{0.9})O_3$ ceramic is detected. The dielectric behavior of $(1-y)Ba(Zr_{0.1}Ti_{0.9})O_3-yBa(Zn_{1/3}Nb_{2/3})O_3$ ceramics can be easily distinguished from that of the pure $Ba(Zr_{0.1}Ti_{0.9})O_3$ ceramic when $T<T_m$. The $\varepsilon_r$ (in the range of $T<T_m$) and especially the permittivity maximum of BZT−BZN ceramics decreases obviously with the increase of test frequency, as indicated in Figs. 3(b−f). The frequency dispersion of $\varepsilon_{r,max}$ clearly demonstrates a relaxation nature, namely a relaxor-type permittivity, for $(1-y)Ba(Zr_{0.1}Ti_{0.9})O_3-yBa(Zn_{1/3}Nb_{2/3})O_3$ ceramics. The dielectric loss of all BZT−BZN samples also shows obvious frequency-dependent characteristics.

The $T_m$ for BZT−BZN samples moves toward higher temperatures with increasing frequency. The empirical relaxation strength describing the frequency dispersion of $T_m$ is defined as [7,14]

$$\Delta T_{rs}=T_{m(500\ kHz)}-T_{m(1\ kHz)} \tag{1}$$

The values of $\Delta T_{rs}$ and $T_m$ at different frequencies for BZT−BZN samples are given in Table 3. The $\Delta T_{rs}$ increases from 2 °C for $0.99Ba(Zr_{0.1}Ti_{0.9})O_3-0.01Ba(Zn_{1/3}Nb_{2/3})O_3$ ceramic to 10 °C for $0.95Ba(Zr_{0.1}Ti_{0.9})O_3-0.05Ba(Zn_{1/3}Nb_{2/3})O_3$ ceramic, indicating an enhanced frequency dispersion of $T_m$ in BZT−BZN ceramics with the increase of $y$.

**Table 3** $\Delta T_{rs}$ and $T_m$ at different frequencies for $(1-y)Ba(Zr_{0.1}Ti_{0.9})O_3-yBa(Zn_{1/3}Nb_{2/3})O_3$ ceramics

| $y$ | $T_m$/°C | | | | | | $\Delta T_{rs}$/°C |
|---|---|---|---|---|---|---|---|
| | 200 Hz | 1 kHz | 10 kHz | 100 kHz | 250 kHz | 500 kHz | |
| 0 | 93 | 93 | 93 | 93 | 93 | 93 | 0 |
| 0.01 | 57 | 57 | 57 | 59 | 59 | 59 | 2 |
| 0.02 | 37 | 37 | 39 | 39 | 39 | 39 | 2 |
| 0.03 | 21 | 21 | 21 | 23 | 23 | 23 | 2 |
| 0.04 | −2.7 | −2.7 | −0.8 | −0.8 | −0.8 | 1.4 | 4.1 |
| 0.05 | −91 | −89 | −87 | −81 | −79 | −79 | 10 |

### 3.4 Diffuse phase transition

In order to describe the broadening in $\varepsilon_r-T$ curve, the full-width of half-maximum (FWHW) of $\varepsilon_r-T$ curve at 1 kHz is calculated here. The FWHW increases from ~47 °C (from 69 to 116 °C) for pure $Ba(Zr_{0.1}Ti_{0.9})O_3$ sample to ~94 °C (from −14 to 80 °C) for $0.98Ba(Zr_{0.1}Ti_{0.9})O_3-0.02Ba(Zn_{1/3}Nb_{2/3})O_3$ sample and ~181 °C (from −111 to 70 °C) for the $0.96Ba(Zr_{0.1}Ti_{0.9})O_3-0.04Ba(Zn_{1/3}Nb_{2/3})O_3$ sample. With increasing $y$, the Curie peak of $(1-y)Ba(Zr_{0.1}Ti_{0.9})O_3-yBa(Zn_{1/3}Nb_{2/3})O_3$ ceramics becomes more broadened, suggesting a diffuse phase transition around $T_m$. Besides the flattening of the dielectric constant ($\varepsilon_r$) versus temperature ($T$) curve previously mentioned, the diffuse phase transition is also characterized by a huge separation in temperature between the maximum of the real (dielectric constant) and imaginary (dielectric loss) parts of the dielectric spectrum, as indicated in Fig. 3.

The modified Curie−Weiss law is utilized to describe the diffuseness of the ferroelectric phase transition as well [21]:

$$\frac{1}{\varepsilon_r}-\frac{1}{\varepsilon_{r,max}}=\frac{(T-T_m)^{\gamma}}{C'} \tag{2}$$

where $\gamma$ and $C'$ are assumed to be constants. The parameter $\gamma$ (commonly between 1 and 2) describes the characteristic of the phase transition. When $\gamma$ equals 1, a normal Curie−Weiss law is obtained. At the other extreme ($\gamma$=2), a complete diffuse phase transition is described. The parameters $\gamma$ can be determined by the slope after linear fitting the data through $\ln(1/\varepsilon_r-1/\varepsilon_{r,max})-\ln(T-T_m)$. The plots of $\ln(1/\varepsilon_r-1/\varepsilon_{r,max})$ as a function of $\ln(T-T_m)$ for $(1-y)Ba(Zr_{0.1}Ti_{0.9})O_3-yBa(Zn_{1/3}Nb_{2/3})O_3$ ceramics are shown in Fig. 4. The $\gamma$ value increases as the $y$ increases, clearly indicating that the $(1-y)Ba(Zr_{0.1}Ti_{0.9})O_3-yBa(Zn_{1/3}Nb_{2/3})O_3$ ceramics exhibit an enhanced diffuse ferroelectric−paraelectric phase transition behavior with the increase of $Ba(Zn_{1/3}Nb_{2/3})O_3$ content.

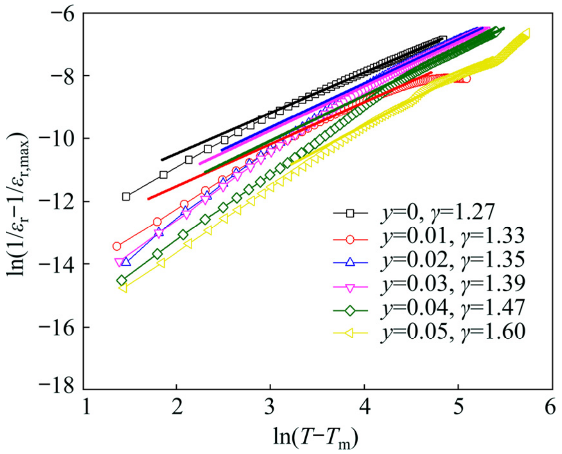

**Fig. 4** Plots of $\ln(1/\varepsilon_r-1/\varepsilon_{r,max})$ as function of $\ln(T-T_m)$ for $(1-y)Ba(Zr_{0.1}Ti_{0.9})O_3-yBa(Zn_{1/3}Nb_{2/3})O_3$ ceramics at 1 kHz

Since there is no frequency dispersion of $\varepsilon_r$ and $T_m$, a normal ferroelectric behavior accompanied by diffuse phase transition is obtained for pure $Ba(Zr_{0.1}Ti_{0.9})O_3$ ceramic. However, $Ba(Zr_{0.1}Ti_{0.9})O_3$ ceramics with high $Ba(Zn_{1/3}Nb_{2/3})O_3$ content exhibit the typical relaxor-like ferroelectric behavior with a strong frequency dispersion of $\varepsilon_r$ at $T<T_m$ and a strong diffuse phase transition. Moreover, the diffuse transition behavior and the frequency dispersion are enhanced with increasing $Ba(Zn_{1/3}Nb_{2/3})O_3$ content, implying a composition-induced relaxor ferroelectric behavior.

### 3.5 Dielectric properties

Due to the above-mentioned intensified diffuse phase transformation, the temperature stability of permittivity is expected to be improved. For characterizing this property, the permittivity variation ($\Delta\varepsilon_r/\varepsilon_r$) (from −30 to 85 °C and from −55 to 125 °C) at 1 kHz determined using the following equation is calculated:

$$\Delta\varepsilon_r/\varepsilon_r=\frac{\varepsilon_{r,T}-\varepsilon_{r,RT}}{\varepsilon_{r,RT}}\times 100\% \quad (3)$$

where $\varepsilon_{r,RT}$ is the relative dielectric constant at room temperature (25 °C) and $\varepsilon_{r,T}$ is the relative dielectric constant at any other temperature.

The $\varepsilon_{r,RT}$, $\varepsilon_{r,max}$, $\Delta\varepsilon_r/\varepsilon_r$ and the dielectric loss at room temperature ($\tan\delta_{RT}$) are collected in Table 4. It is obvious that the $\varepsilon_{r,RT}$ and the $\tan\delta_{RT}$ increase initially and then decrease as $y$ increases. The $0.96Ba(Zr_{0.1}Ti_{0.9})O_3-0.04Ba(Zn_{1/3}Nb_{2/3})O_3$ sample exhibits moderate relative dielectric constant and dielectric loss at room temperature. The $\varepsilon_{r,max}$ is suppressed from 8948 to 1611 as $y$ increases from 0 to 0.05, which is attributed to the complex occupation of aliovalent ions in $B$ sites of perovskite structure. The $\Delta\varepsilon_r/\varepsilon_r$ of $Ba(Zr_{0.1}Ti_{0.9})O_3$ is also suppressed after being combined with $Ba(Zn_{1/3}Nb_{2/3})O_3$, approaching the X7R standard ($\Delta\varepsilon_r/\varepsilon_r\le\pm 15\%$ from −55 to 125 °C) [21] according to the Electronic Industries Association (EIA) as $y$ increases. Although the present BZT−BZN ceramics still do not satisfy the X7R Standard, some of them are suitable for the Y5V ($\Delta\varepsilon_r/\varepsilon_r\le 22\%-(-82\%)$ from −30 to 85 °C) ceramic capacitor applications.

The $T_m$ of BZT−BZN ceramics decreases significantly with the increase of $Ba(Zn_{1/3}Nb_{2/3})O_3$ content (see Table 3), indicating that the $Ba(Zn_{1/3}Nb_{2/3})O_3$, actually the lattice deformation resulting from the $B$ site occupation of $Zn^{2+}$ and $Nb^{5+}$ ions in BZT ceramics, can remarkably influence the ferroelectric−paraelectric phase transition temperature of present system.

### 3.6 Ferroelectric properties

Figure 5 shows the ferroelectric hysteresis loops of $(1-y)Ba(Zr_{0.1}Ti_{0.9})O_3-yBa(Zn_{1/3}Nb_{2/3})O_3$ ceramics at room temperature. The $P-E$ loops for samples with $y$=0 or 0.01 confirm the ferroelectric nature of pure $Ba(Zr_{0.1}Ti_{0.9})O_3$ ceramics and BZT−BZN ceramics with low $Ba(Zn_{1/3}Nb_{2/3})O_3$ contents. However, the almost linear $P-E$ curves for samples with $y$=0.04 or 0.05 as illustrated in Fig. 5 indicate the paraelectric nature of $Ba(Zr_{0.1}Ti_{0.9})O_3$ceramics with high $Ba(Zn_{1/3}Nb_{2/3})O_3$ contents. This demonstrates that the $(1-y)Ba(Zr_{0.1}Ti_{0.9})O_3-yBa(Zn_{1/3}Nb_{2/3})O_3$ ceramics transit from ferroelectric to paraelectric phase at room temperature with increasing $y$, which consists with the result revealed by the decreasing of $T_m$.

The remnant polarization ($2P_r$) and coercive field ($2E_c$) of $(1-y)Ba(Zr_{0.1}Ti_{0.9})O_3-yBa(Zn_{1/3}Nb_{2/3})O_3$ ceramics are given in Table 5. The remnant polarization decreases obviously with

**Table 4** Dielectric parameters for $(1-y)Ba(Zr_{0.1}Ti_{0.9})O_3-yBa(Zn_{1/3}Nb_{2/3})O_3$ ceramics at 1 kHz

| $y$ | $\varepsilon_{r,RT}$ | $\tan\delta_{RT}$ | $\varepsilon_{r,max}$ | $(\Delta\varepsilon_r/\varepsilon_r)$/% ((−30)−85 °C) | $(\Delta\varepsilon_r/\varepsilon_r)$/% ((−55)−125 °C) |
|---|---|---|---|---|---|
| 0 | 1370 | 0.021 | 8948 | (+449.6)−(−56.6) | (+553.1)−(−67.4) |
| 0.01 | 5167 | 0.055 | 7392 | (+43.1)−(−55.2) | (+43.1)−(−68.3) |
| 0.02 | 6166 | 0.017 | 6679 | (+8.3)−(−57.6) | (+8.3)−(−75.2) |
| 0.03 | 6076 | 0.0097 | 6110 | (+0.56)−(−63.8) | (+0.56)−(−78.7) |
| 0.04 | 3780 | 0.0081 | 4237 | (+12.1)−(−54.2) | (+12.1)−(−68.8) |
| 0.05 | 1135 | 0.0048 | 1611 | (+26.4)−(−15.9) | (+35.9)−(−23.3) |

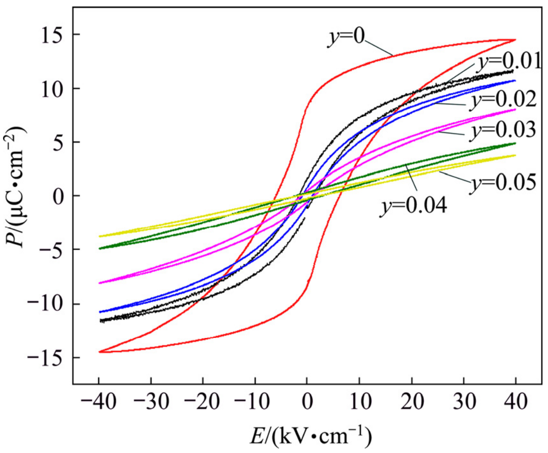

**Fig. 5** Ferroelectric hysteresis loops of $(1-y)Ba(Zr_{0.1}Ti_{0.9})O_3-yBa(Zn_{1/3}Nb_{2/3})O_3$ ceramics at room temperature

**Table 5** $2P_r$ and $2E_c$ values for $(1-y)Ba(Zr_{0.1}Ti_{0.9})O_3-yBa(Zn_{1/3}Nb_{2/3})O_3$ ceramics

| $y$ | $2P_r/(\mu C\cdot cm^{-2})$ | $2E_c/(kV\cdot cm^{-1})$ |
|---|---|---|
| 0 | 16.72 | 12.26 |
| 0.01 | 2.8 | 3.03 |
| 0.02 | 1.39 | 1.95 |
| 0.03 | 1.06 | 2.41 |
| 0.04 | 0.72 | 4.86 |
| 0.05 | 0.45 | 3.99 |

increasing $Ba(Zn_{1/3}Nb_{2/3})O_3$ content. The coercive field of BZT−BZN ceramics initially decreases remarkably with the increase of $y$ and then increases slightly. The $P_r$ and $E_c$ are commonly used for characterizing the ferroelectric properties and are strongly depended on grain size, phase transition and some other factors like defect concentration [10,22,23]. The ceramics with large grains prefer to exhibit larger $P_r$ and lower $E_c$ [24]. The smaller grains in ferroelectric ceramics restrict the formation of large ferroelectric domains and thus reduce the effective contribution to total polarization [25]. Also, it is more difficult for the reversal polarization of a ferroelectric domain inside a small grain than in a large one [22]. Therefore, the above-mentioned decrease of the average grain size with increasing $y$ leads to the decrease of $P_r$ as well as the increase of $E_c$. The increasing amount of paraelectric phase in BZT ceramics commonly results in a smaller $P_r$ [26]. The ferroelectric−paraelectric phase transition in the present concerned BZT−BZN ceramics with increasing $Ba(Zn_{1/3}Nb_{2/3})O_3$ content also contributes to the decrease of $P_r$ and $E_c$. Obviously, the variation of $E_c$ with increasing $y$ value is determined by the competitive result between the decreasing grain size and the increasing amount of paraelectric phase.

## 4 Conclusions

(1) The BZT−BZN ceramic is a single phase solid solution with perovskite structure as $y$ increases up to 0.05.

(2) The average grain size of BZT−BZN ceramics decreases from 54.27 to 1.12 μm with the increase of $Ba(Zn_{1/3}Nb_{2/3})O_3$ content.

(3) The $T_m$ of BZT-BZN ceramics is shifted to lower temperature by increasing the $Ba(Zn_{1/3}Nb_{2/3})O_3$ content. The permittivity variation is suppressed with increasing $y$. According to the increase of critical exponent $\gamma$ from the modified Curie−Weiss law, the composition-induced diffuse phase transition behavior of BZT−BZN ceramics is enhanced with increasing $Ba(Zn_{1/3}Nb_{2/3})O_3$ content.

(4) The relaxor-like ferroelectric behavior with a strong frequency dispersion of $T_m$ and $\varepsilon_r$ at $T<T_m$ accompanied by a strong diffuse phase transition is found for BZT−BZN ceramics with high $Ba(Zn_{1/3}Nb_{2/3})O_3$ content.

(5) Due to the decreased grain size and the increased amount of paraelectric phase, the remnant polarization of BZT−BZN ceramics decreases with increasing $y$, while the coercive field decreases remarkably and then increases with the increase of $Ba(Zn_{1/3}Nb_{2/3})O_3$ content.

## Acknowledgments

This work is sponsored by the National Demonstration Center for Experimental Materials Science and Engineering Education (Jiangsu University of Science and Technology, China). This work is also funded by the Priority Academic Program Development (PAPD) of Jiangsu Higher Education Institutions, China.

## References

[1] ZHANG Li-hua, WANG Shu-lin, LIU Fang-hua. Effect of Eu doping on the structural, electrical, and dielectric properties of $K_{0.5}Na_{0.5}NbO_3$ ceramics for high-temperature

capacitor applications [J]. Journal of Electronic Materials, 2015, 44: 3408−3414.

[2] LU Da-yong, SUN Xiu-yun, TODA M. A novel high-*k* 'Y5V' barium titanate ceramics co-doped with lanthanum and cerium [J]. Journal of Physics and Chemistry of Solids, 2007, 68: 650−664.

[3] LI M, PIETROWSKI M J, de SOUZA R A, ZHANG H, REANEY I M, COOK S N, KILNER J A, SINCLAIR D C. A family of oxide ion conductors based on the ferroelectric perovskite $Na_{0.5}Bi_{0.5}TiO_3$ [J]. Nature Materials, 2014, 13: 31−35.

[4] ZHANG Chen, CHEN Fang-xu, LING Zhi-xin, JIAN Gang, LI Yuan-liang. Microstructure and dielectric properties of $La_2O_3$ doped Ti-rich barium strontium titanate ceramics for capacitor applications [J]. Materials Science−Poland, 2017, 35: 806−815.

[5] HAN Ru-qu, DONG Song-tao, WANG Yuan-xiang, LI Xiao-xi, ZHANG Ya-mei. Electrical and oxygen sensing properties of $Nd_{1-x}Ba_xCoO_3$ ceramics [J]. Journal of Materials Science: Materials in Electronics, 2017, 28: 14234−14239.

[6] MORRISON F D, SINCLAIR D C, WEST A R. Electrical and structural characteristics of lanthanum-doped barium titanate ceramics [J]. Journal of Applied Physics, 1999, 86: 6355−6366.

[7] ZHANG Chen, CHEN Fang-xu, ZHONG Xin, LING Zhi-xin, TANG Zhu-ming, JIAN Gang. Enhanced ferroelectric relaxor behavior of $Ho_2O_3$-modified barium zirconate titanate ceramics [J]. Journal of Materials Science: Materials in Electronics, 2018, 29: 16730−16739.

[8] WANG Yan, CUI Bin, ZHANG Lu-lu, HU Zhen-yu, WANG Yao-yu. Phase composition, microstructure, and dielectric properties of dysprosium-doped $Ba(Zr_{0.1}Ti_{0.9})O_3$-based Y5V ceramics with high permittivity [J]. Ceramics International, 2014, 40: 11681−11688.

[9] CHOU Xiu-jian, ZHAI Ji-wei, JIANG Hai-tao, YAO Xi. Dielectric properties and relaxor behavior of rare-earth (La, Sm, Eu, Dy, Y) substituted barium zirconium titanate ceramics [J]. Journal of Applied Physics, 2007, 102: 084106.

[10] SANGWAN K M, AHLAWAT N, KUNDU R S, RANI S, RANI S, AHLAWAT N, MURUGAVEL S. Improved dielectric and ferroelectric properties of Mn doped barium zirconium titanate (BZT) ceramics for energy storage applications [J]. Journal of Physics and Chemistry of Solids, 2018, 117: 158−166.

[11] KUANG S J, TANG X G, LI L Y, JIANG Y P, LIU Q X. Influence of Zr dopant on the dielectric properties and Curie temperatures of $Ba(Zr_xTi_{1-x})O_3$ ($0 \le x \le 0.12$) ceramics [J]. Scripta Materialia, 2009, 61: 68−71.

[12] WEBER U, GREUEL G, BOETTGER U, WEBER S, HENNINGS D, WASER R. Dielectric properties of $Ba(Zr,Ti)O_3$-based ferroelectrics for capacitor applications [J]. Journal of the American Ceramic Society, 2001, 84: 759−766.

[13] HENNINGS D, SCHNELL A, SIMON G. Diffuse ferroelectric phase transitions in $Ba(Ti_{1-y}Zr_y)O_3$ ceramics [J]. Journal of the American Ceramic Society, 1982, 65: 539−544.

[14] TANG X G, CHEW K H, CHAN H L W. Diffuse phase transition and dielectric tunability of $Ba(Zr_yTi_{1-y})O_3$ relaxor ferroelectric ceramics [J]. Acta Materialia, 2004, 52: 5177−5183.

[15] BADAPANDA T. Glassy behavior study of dysprosium doped barium zirconium titanate relaxor ferroelectric [J]. Journal of Advanced Ceramics, 2014, 3: 339−348.

[16] BADAPANDA T, ROUT S K, CAVALCANTE L S, SCZANCOSKI J C, PANIGRAHI S, SINHA T P, LONGO E. Structural and dielectric relaxor properties of yttrium-doped $Ba(Zr_{0.25}Ti_{0.75})O_3$ ceramics [J]. Materials Chemistry and Physics, 2010, 121: 147−153.

[17] DIEZ-BETRIU X, GARCIA J E, OSTOS C, BOYA A U, OCHOA D A, MESTRES L, PEREZ R. Phase transition characteristics and dielectric properties of rare-earth (La, Pr, Nd, Gd) doped $Ba(Zr_{0.09}Ti_{0.91})O_3$ ceramics [J]. Materials Chemistry and Physics, 2011, 125: 493−499.

[18] BHARGAVI G N, KHARE A, BADAPANDA T, RAY P K, BRAHME N. Influence of Eu doping on the structural, electrical and optical behavior of barium zirconium titanate ceramic [J]. Ceramics International, 2018, 44: 1817−1825.

[19] WANG Yong-li, LI Long-tu, QI Jian-quan, GUI Zhi-lun. Ferroelectric characteristics of ytterbium-doped barium zirconium titanate ceramics [J]. Ceramics International, 2002, 28: 657−661.

[20] JARUPOOM P, JAITA P, BOOTHRAWONG N, PHATUNGTHANE T, SANJOOM R, RUJIJANAGUL G, CANN D P. Influence of CoO nanoparticles on properties of barium zirconium titanate ceramics [J]. Journal of Electronic Materials, 2017, 46: 4267−4275.

[21] ZHANG Chen, CHEN Fang-xu, LING Zhi-xin, ZHONG Xin, JIAN Gang, LI Yuan-liang. The dielectric properties and diffuse phase transition of nonstoichiometric barium strontium titanate based capacitor ceramics [J]. Journal of Materials Science: Materials in Electronics, 2018, 29: 9397−9405.

[22] CAI Wei, FU Chun-lin, LIN Ze-bin, DENG Xiao-ling. Vanadium doping effects on microstructure and dielectric properties of barium titanate ceramics [J]. Ceramics International, 2011, 37: 3643−3650.

[23] CHEN Jian, FU Chun-lin, CAI Wei, CHEN Gang, RAN Shao-nian. Microstructures, dielectric and ferroelectric properties of $BaHf_xTi_{1-x}O_3$ ceramics [J]. Journal of Alloys and Compounds, 2012, 544: 82−86.

[24] SUN Hua-jun, ZHANG Yong, LIU Xiao-fang, LIU Yi, CHEN Wen. Effects of CuO additive on structure and electrical properties of low-temperature sintered $Ba_{0.98}Ca_{0.02}Zr_{0.02}Ti_{0.98}O_3$ lead-free ceramics [J]. Ceramics International, 2015, 41: 555−565.

[25] ZHAI Ji-wei, YAO Xi, SHEN Jun, ZHANG Liang-Ying, CHEN H. Structural and dielectric properties of Ba($Zr_xTi_{1-x}$)$O_3$ thin films prepared by the sol-gel process [J]. Journal of Physics D: Applied Physics, 2004, 37: 748−752.

[26] CAI Wei, FU Chun-lin, GAO Jia-cheng, LIN Ze-bin, DENG Xiao-ling. Effect of hafnium on the microstructure, dielectric and ferroelectric properties of Ba[$Zr_{0.2}Ti_{0.8}$]$O_3$ ceramics [J]. Ceramics International, 2012, 38: 3367−3375.

# $(1-y)Ba(Zr_{0.1}Ti_{0.9})O_3-yBa(Zn_{1/3}Nb_{2/3})O_3$ 陶瓷的介电性能及弛豫铁电行为

钟 鑫，张 晨，陈方旭，唐柱明，简 刚

江苏科技大学 材料科学与工程学院，镇江 212002

**摘 要：**采用传统固相法制备$(1-y)Ba(Zr_{0.1}Ti_{0.9})O_3-yBa(Zn_{1/3}Nb_{2/3})O_3$ ($y$=0~0.05)陶瓷，利用 XRD、 SEM、电参数测试系统以及铁电测试仪研究其显微结构、介电性能及铁电行为。结果表明：随着 $y$ 增大至 0.05，该锆钛酸钡基陶瓷始终为单相钙钛矿结构，其平均晶粒尺寸随 $y$ 的增大而减小。介电常数最大值 $\varepsilon_{r,max}$ 在 1 kHz 下随 $y$ 增大从 8948 显著降低至 1611，且其铁电−顺电相变温度 $T_m$ 亦随 $y$ 增大从 93 °C 降低至−89 °C。该陶瓷成分诱导弥散相变随 $y$ 增大而逐渐增强。高 $y$ 取值下陶瓷表现出以 $T_m$ 及铁电温区介电常数的强烈频率色散及弥散相变为典型特征的弛豫铁电行为。该陶瓷体系的剩余极化强度随 $y$ 增大而降低，而矫顽场则在显著降低后有所提高。

**关键词：**锆钛酸钡；介电性能；弛豫铁电行为；钙钛矿；相变

**(Edited by Bing YANG)**